fractal and fractional

MDPI

Article

Lagrangian Particle Dispersion in a Poor Man's Magnetohydrodynamic Turbulence Model

Tommaso Alberti [1,*] and Vincenzo Carbone [2]

[1] Istituto Nazionale di Geofisica e Vulcanologia, Via di Vigna Murata 605, 00143 Roma, Italy
[2] Dipartimento di Fisica, Università della Calabria, Ponte P. Bucci, Cubo 31C, 87036 Rende, Italy; vincenzo.carbone@fis.unical.it
* Correspondence: tommaso.alberti@ingv.it

Abstract: Lagrangian dispersion of fluid particle pairs refers to the study of how individual fluid particles disperse and move in a fluid flow, providing insights to understand transport phenomena in various environments, from laminar to turbulent conditions. Here, we explore this phenomenon in synthetic velocity and magnetic fields generated through a reduced-order model of the magnetohydrodynamic equations, which is able to mimic both a laminar and a turbulent environment. In the case of laminar conditions, we find that the average square distance between particle pairs increases linearly with time, implying a dispersion pattern similar to Brownian motion at all time steps. On the other hand, under turbulent conditions, surprisingly enough we observe a Richardson scaling, indicating a super-ballistic dispersion pattern, which aligns with the expected scaling properties for a turbulent environment. Additionally, our study reveals that the magnetic field plays an organizing role. Lastly, we explore a purely hydrodynamic case without magnetic field effects, showing that, even in a turbulent environment, the behavior remains Brownian-like, highlighting the crucial role of the magnetic field in generating the Richardson scaling observed in our model.

Keywords: magnetohydrodynamic turbulence; Lagrangian dispersion; dynamical systems

Citation: Alberti, T.; Carbone, V. Lagrangian Particle Dispersion in a Poor Man's Magnetohydrodynamic Turbulence Model. *Fractal Fract.* **2023**, *7*, 662. https://doi.org/10.3390/fractalfract7090662

Academic Editor: Carlo Cattani

Received: 15 August 2023
Revised: 29 August 2023
Accepted: 29 August 2023
Published: 31 August 2023

1. Introduction

Magnetohydrodynamic (MHD) turbulence is a fascinating and complex phenomenon that occurs both in astrophysical and laboratory plasma environments where magnetic fields and fluid flows actively interact [1,2]. Understanding MHD turbulence is crucial for unraveling the behavior of various cosmic objects, such as stars, accretion disks, and galaxies, as well as for advancing the field of fusion energy, e.g., [3–6]. The study of MHD turbulence combines theoretical, computational, and experimental approaches. Numerical simulations based on MHD equations provide valuable insights into the complex interplay between fluid motions and magnetic fields, e.g., [7–9]. Experimental investigations in laboratory devices, such as magnetized plasma devices or liquid metal experiments, offer the opportunity to probe the intricate dynamics of MHD turbulence under controlled conditions, e.g., [10,11]. Theoretical models and analytical techniques, including statistical theories and spectral analysis, provide frameworks to understand the fundamental aspects of MHD turbulence and predict its behavior in different regimes, e.g., [2,12–16]. Despite the significant progress that has been made in advancing our understanding of MHD turbulence in recent years, many challenges remain, such as the role of turbulence in energizing/accelerating neutral and charged particles, which is important for many applications, e.g., [17,18].

Turbulence is usually described in the Eulerian framework, i.e., from the point of view of a still observer, and in a statistical way, i.e., by searching for high-order statistics of fluctuations at a given scale, e.g., [19–21]. The scaling of fluctuations accounts for spatial intermittency in the turbulence cascade, which implies, statistically, non-Gaussian tails

for the probability distributions of both velocity and magnetic field increments, leading to abrupt energizations/accelerations of particles. Similar considerations can be drawn for Lagrangian turbulence, e.g., [22,23], where a universal form can be retrieved for a locally averaged energy transfer rate along particle trajectories. Nevertheless, the Lagrangian statistic is still intermittent, thus questioning how it affects the dispersion of particles [24].

Due to the inherent complexity and multi-scale behavior of turbulence, it is widely approached from a reduced-order modeling point of view, such as that for cascade models, which provides a valuable and relatively simple framework for understanding the energy transfer processes and the emergence of different scales in fluid and MHD turbulence [25–29]. These models describe the transfer of energy from large-scale structures to smaller scales through a series of cascades, capturing the essential dynamics of MHD turbulence, ultimately determining the distribution of energy and the formation of coherent structures in the turbulent flow. Cascade models can be seen as a low-order description of the MHD equations following some prescribed rules on the coupling between the different scales, generally relying on the so-called triad interactions [25,29]. An even more simplified low-order model, known as poor man's MHD equations, has been recently derived by Alberti et al. [13]. It captures the essential behavior of magnetohydrodynamics in a reduced form and can be used as a simplified model to study certain aspects of MHD systems while neglecting certain complexities. Despite its simplifications, the PMMHD model is able to preserve the total energy in the ideal MHD approximation to recover all fixed points of the usual MHD equations, to reproduce a kinematic dynamo action, and to show a Kolmogorov-like spectral scaling, as expected for turbulent plasmas [2,13].

In this paper, we exploit Lagrangian particle dispersion in synthetic velocity and magnetic fields generated via the PMMHD model under both laminar and turbulent conditions. We show that under laminar conditions the average square distance between particle pairs behaves linearly in time, thus suggesting a Brownian-like dispersion for all time steps. Conversely, under turbulent conditions, a Richardson scaling, corresponding to a super-ballistic dispersion, is observed, in agreement with the scaling properties expected for a turbulent environment. Indeed, the observed scaling is observed along the inertial sub-range of turbulence reproduced by the PMMHD model. We also show that the magnetic field is much more efficient in dispersing particle pairs with respect to the velocity one in a turbulent environment, while no differences are found for a laminar one. However, stronger anisotropies are generated by the velocity field with respect to the magnetic one, thus suggesting an ordering role of the magnetic field. Finally, by exploiting a purely hydrodynamic case (with no magnetic field effects) we show that, also for a turbulent environment, a Brownian-like behavior is observed, thus pointing out a key role of the magnetic field in generating a Richardson scaling. This paper is organized as follows. Section 2 describes the suitable theoretical framework for Lagrangian dispersion, while Section 3 briefly recaps the PMMHD model. Then, in Section 4, we present our Lagrangian model setup to inspect the dispersion of particles in laminar and turbulent fields generated via the PMMHD model under three different scenarios: velocity dispersion (Section 5), alfvénic dispersion (Section 6), and purely hydrodynamic dispersion (Section 7). Finally, we summarize our results and possible future outlooks in Section 8.

2. Lagrangian Dispersion of Particle Pairs

Particle pair separation in a turbulent environment is a classical issue of fluid flows [30], which is important not only from a theoretical point of view, but even for practical issues [31]. In MHD turbulence, this is not yet well-established, in particular the existence of a Richardson law. Numerical simulations have been widely used to describe pair dispersion properties [32], although it is interesting to use turbulent environments AND not direct numerical simulations to verify the robustness of the classical laws for pair dispersion. This is particularly true for MHD turbulence, where anisotropy cannot be ruled out.

The main variable we can investigate [30] is the concentration $\theta(\mathbf{x},t)$ of a cloud of particles at the time t, so that we can define a continuous function $q(\mathbf{r},t)$ as the relative number of particle pairs whose coordinates differ by an amount $\mathbf{r}$

$$q(\mathbf{r},t) = \int \theta(\mathbf{x},t)\theta(\mathbf{x}+\mathbf{r},t)d\mathbf{x}, \tag{1}$$

normalized in a way that the integral over all pairs of $q(\mathbf{r},t)$ is equal to one. The dispersive process can then be fully described through the probability that, given $q_0(\mathbf{r}_0)$, the averaged concentration at the time $t=0$, we recover the concentration at a time t, namely

$$q(\mathbf{r},t) = \int p(\mathbf{r}|\mathbf{r}_0,t)q_0(\mathbf{r}_0)d\mathbf{r}_0 \tag{2}$$

However, the determination of the probability requires the estimate of the quantity $q(\mathbf{r},t)$, which could be quite difficult from experiments or numerical simulations. As an alternative, we can estimate the components of the relative dispersion tensor $\ell_{ij}(t)$. Given a cloud of N particles which move dispersively within a fluctuating environment, for every pair of particles, (n,m), identified at time t by the coordinates $\mathbf{X}^{(n)}(t)$ and $\mathbf{X}^{(m)}(t)$, we calculate the relative distance $\Delta_i^{(n,m)}(t) = X_i^{(n)}(t) - X_i^{(m)}(t)$ along each direction, thus defining the dispersion tensor as

$$\ell_{ij}(t) = \langle \Delta_i^{(n,m)}(t)\Delta_j^{(n,m)}(t)\rangle \tag{3}$$

where brackets means average over all $N(N-1)/2$ particle pairs. In an isotropic situation where every direction plays the same role, then the out-of-diagonal elements of the tensor are, in principle, identically zero and the trace of the tensor $\ell^2(t) = \ell_{ii}$ represents the average radius of the cloud of particles at the time t, being $\ell_{xx} \simeq \ell_{yy} \simeq \ell_{zz}$. In this case, we can define an effective eddy diffusivity $K(\ell,t)$ for the cloud.

Assuming that the eddy diffusivity must depend solely on the average energy dissipation rate ϵ and on the length scale ℓ, it immediately follows that the eddy diffusivity is related to the trace of the dispersion tensor through the celebrated Richardson fourth-third law [33,34]

$$K(\ell,t) = K_0\epsilon\ell^{4/3} \tag{4}$$

By defining an eddy diffusivity equation $d\ell^2(t)/dt = 6K(\ell,t)$, it follows that particle pairs separate in time following a super-ballistic law

$$\ell^2(t) = g\epsilon t^3 \tag{5}$$

where g is a constant. Both fundamental laws (4) and (5) have been verified in fluid flows and numerical simulations [23,24,31,34]. As an important consequence, since $\ell(t)$ is obviously related to the turbulent velocity fluctuations δu_ℓ across eddies at that scale $d\ell/dt \sim \delta u_\ell$, it follows that scaling property (4) requires a turbulent environment with a Kolmogorov scaling $\delta u_\ell \sim \ell^{1/3}$ saying the Richardson pair dispersion law is valid in the inertial sub-range of turbulence.

The Richardson law is an asymptotic property of dispersion within the inertial sub-range of turbulence, where particles lost memory of their infinitesimal initial separation $\Delta_i^{n,m}(0)$ [34]. This is a rough approximation, as shown in some recent papers [35–37]. We can introduce a revised version of the model by conjecturing instead that the eddy-diffusivity must depend on the initial pair average separation, say, ℓ_0, on the average dissipation rate ϵ, and explicitly on time, so that the eddy diffusivity can assume a more generic form

$$K(\ell,t) = K_0\ell_0^\alpha\epsilon^\beta t^\zeta \tag{6}$$

Dimensional arguments lead to $\alpha = 2-(\zeta+1)/3$ and $\beta = (\zeta+1)/3$, where ζ is arbitrary. By assuming a quadratic dependence of the eddy diffusivity on time, say, $\zeta = 2$,

we recover the Richardson's law. However, according to the considerations by Elsinga et al. [37], if we assume a linear dependence on time, it follows that

$$K(\ell, t) = K_0(\epsilon \ell_0)^{2/3} t \tag{7}$$

which means a ballistic separation of particle pairs

$$\ell^2(t) = g_1 \epsilon^{2/3} t^2 \tag{8}$$

This corresponds to the Batchelor's law of particle pair dispersion, and is valid for times less than, say, t_0, the eddy-turnover-time at the scale ℓ_0. On the contrary, the Richardson law is valid in the intermediate range of times $t_0 \ll t \ll t_L$, with t_L being the large-scale eddy-turnover-time [37], or the time needed for the particle to loose memory of the initial conditions. As particles separate enough, say, for $t \gg t_L$, they decorrelate, so that they must evolve without any correlation and the eddy diffusivity must be constant, say, $\zeta = 0$, thus obtaining a Brownian-like Taylor's dispersion

$$\ell^2(t) = g_2 \epsilon^{1/3} t. \tag{9}$$

3. The Poor Man's Magnetohydrodynamic (PMMHD) Model

In the low-frequency approximation, fluctuations in plasmas are usually described in an incompressible framework via the MHD equations, which read as

$$\partial_t u_i = -u_j \partial_j u_i - \partial_i \left(c_s^2 + c_A^2 \right) + b_j \partial_j b_i + \nu \partial^2 u_i, \tag{10}$$

$$\partial_t b_i = -u_j \partial_j b_i + b_j \partial_j u_i + \eta \partial^2 b_i, \tag{11}$$

$$\partial_i u_i = \partial_j b_j = 0, \tag{12}$$

with $u_i(\mathbf{r}, t)$ and $b_i(\mathbf{r}, t)$ being the velocity and magnetic fields, respectively, c_s and c_A the sound and Alfvén speeds, ν and η the kinematic viscosity and magnetic diffusivity, respectively, and we assumed, for simplicity, a unitary mass density $\rho_0 = 1$. Equation (10) describes the collective motion of a plasma in a single-fluid approximation (ions are inertial, electrons are at rest) and Equation (11) is the induction equation derived from the Maxwell–Faraday law, while Equation (12) is the incompressibility condition for both fields.

Equations (10) and (11) can be projected over a divergence-free space, without loss of generality, by using the Leray operator that allows us to neglect the term $\partial_i \left(c_s^2 + c_A^2 \right)$. Then, by using dimensionless variables and by adopting a Galerkin truncation retaining a single fixed wavevector [38], Alberti et al. [13] derived the poor man's magnetohydrodynamic (PMMHD) model

$$\dot{u}_i = \beta_i u_i + \Gamma_i^j \left(b_i b^j - u_i u^j \right), \tag{13}$$

$$\dot{b}_i = \alpha_i b_i + \gamma_i^j \left(u_i b^j - b_i u^j \right), \tag{14}$$

where (non-)dotted variables refer to the value at the time $(t_n)t_{n+1}$.

Equations (13) and (14) constitute a six-dimensional autonomous dynamical system with 12 bifurcation parameters, β_i, α_i, and γ_i^j, which can be linked with physically-based quantities. Specifically,

$$\beta_i = 1 - \frac{L}{\ell_i} Re^{-1}, \tag{15}$$

$$\alpha_i = 1 - \frac{L}{\ell_i} Rm^{-1}, \tag{16}$$

with L being the integral scale and ℓ_i the Taylor scale, respectively [13], while Re and Rm are the fluid and magnetic Reynolds numbers, respectively [1]. Thus, β_i and α_i are related

to the nature of the considered plasma, allowing us to describe a laminar environment when $\beta_i, \alpha_i \to 0$ or a turbulent one when $\beta_i, \alpha_i \to 1$ [13]. Furthermore,

$$\gamma_i^j = \partial_j \varphi_i, \tag{17}$$

with $\varphi_i = \{u_i, b_i\}$ [13], represents the directional derivatives of the field components, or, equivalently, is related to field gradients that define the topological space properties [13,38]. They also represent the off-diagonal term of the third-order coupling tensor

$$\Gamma_i^j = \beta_i \delta_j^i + \gamma_i^j = \beta_i \delta_j^i + \partial_i \varphi^j, \tag{18}$$

with the Einstein notation assumed

$$\Gamma_i^j \varphi_i \varphi^j = \varphi_i \sum_{j=1}^{3} (\beta_i \delta_j^i + \gamma_i^j) \varphi^j, \tag{19}$$

Thus, γ_i^j determines the symmetric and/or asymmetric nature of the field gradients, namely that they define the geometry of the system.

Despite its reduced-order representation, it has been shown [13] that the PMMHD model

- preserves MHD invariants in the ideal approximation ($Re, Rm \to \infty$), namely the energy and the helicity;
- admits all fixed points, namely the fluid ($b_i = 0$), the alfvénic ($u_i = \pm b_i$), and the static Taylor force-free ($u_i = 0$ and $b_i = \Omega_i^j b_j$);
- presents a dissipative behavior $\frac{\partial u_j}{\partial u_j'} < 0$ with a signature of chaos (i.e., sensitive dependence on initial conditions while preserving the statistics of both fields);
- displays a Kolmogorov-like spectral scaling $f^{-5/3}$ under turbulent conditions over an inertial sub-range.

4. Lagrangian Formulation of the PMMHD Model

We built-up a Lagrangian model for investigating the dispersion of fluid particle pairs in a velocity and/or magnetic field, generated via the PMMHD model. Note that both velocity and magnetic variables play the same role, b_i being the velocity of alfvénic fluctuations along a given direction. By defining $\mathbf{X}$ as the particle coordinate at the time t_n and $\mathbf{X}'$ as its coordinate at a further time t_{n+1}, we can write the difference of the coordinates of two different particles, say, the n-th and the m-th, along a given direction

$$\Delta \mathbf{X} = \mathbf{X}^{(n)} - \mathbf{X}^{(m)}. \tag{20}$$

The trajectory of each particle evolves according to the equation

$$X_i' = X_i + s_i \tag{21}$$

where s_i is one of the field along a given coordinate, say, $s_i = (u_i, b_i)$, so that the differences in coordinates depends on the field we are investigating, say, $\Delta X_i^{(s)}$. The dispersive properties of particle pairs are then contained in the time evolution of the relative dispersion tensor (see also Equation (3))

$$\sigma_{ij}^{(s_i, s_j)}(t_n) = \langle \Delta X_i^{(s_i)} \Delta X_j^{(s_j)} \rangle \tag{22}$$

where the average is over a large amount of particle pairs at time t_n. The relative dispersion tensor takes into account the possible advection of both kind of fluctuations, say, velocity

and alfvénic, along the three different directions. For example, the chaotic advection of purely velocity elements is described by

$$\sigma_{ij}^{(u,u)} = \langle \Delta X_i^{(u)} \Delta X_j^{(u)} \rangle, \tag{23}$$

while for purely alfvénic elements, we have

$$\sigma_{ij}^{(b,b)} = \langle \Delta X_i^{(b)} \Delta X_j^{b)} \rangle, \tag{24}$$

which both play a privileged role with respect to mixed elements

$$\sigma_{ij}^{(u,b)} = \langle \Delta X_i^{(u)} \Delta X_j^{(b)} \rangle, \tag{25}$$

$$\sigma_{ij}^{(b,u)} = \langle \Delta X_i^{(b)} \Delta X_j^{(u)} \rangle. \tag{26}$$

In the simplest case of isotropic dynamics, the off-diagonal elements are identically zero. In this case, the advection is measured by the square distances between elements, say,

$$\ell_{s_i,s_j}^2 = \sigma_{jj}^{(s_i,s_j)} \tag{27}$$

assuming summation over repeated indices. The anisotropic advection can instead be measured through the anisotropy angles

$$\theta_{ij}^{(s_i,s_j)} = \tan^{-1}\left(\frac{3\sigma_{ij}^{(s_i,s_j)}}{\ell_{s_i,s_j}^2} \right), \tag{28}$$

namely $\theta_{ij}^{(s_i,s_j)} = \pi/4$ in the case of purely isotropic advection.

Our Lagrangian model consists of solving Equation (21) for $M = 10^6$ particles starting from the same initial position, randomly selected, within a circle of radius $\varepsilon = 10^{-3}$, e.g., $X_i(t_0) = X_0 \pm \varepsilon$ when flowing in a plasma environment described by the PMMHD model in Equations (13) and (14). In this way, we can investigate the separation between particle pairs along time, thus allowing a proper evaluation of the dispersion tensor $\sigma_{ij}^{(s_i,s_j)}(t_n)$ and to investigate their statistics under different environmental conditions, as the bifurcation parameters β_i, α_i, and γ_i^j are varied. In particular, we explore the dispersion of particles in a laminar ($\beta_i = 0.1, \alpha_i = 0.1$) and a turbulent ($\beta_i = 0.9, \alpha_i = 0.9$) plasma environment. This corresponds to Reynolds numbers between 10^2 and 10^4, assuming that the ratio between the integral scale L and the Taylor scale ℓ_i is of the order of 10^3 or greater, as in natural plasmas [2]. We investigate both symmetric ($\gamma_i^j = \gamma = 0.1\ \forall i, j$) and asymmetric field gradients ($\gamma_i^j \in [0.1, 0.4]$) generated via the PMMHD model under three different scenarios: velocity dispersion (Section 5), magnetic dispersion (Section 6), and purely hydrodynamic dispersion (Section 7).

5. Fluid Velocity Dispersion

The first case we study is the fluid velocity dispersion, i.e., $s_i = u_i$, of particles. Figure 1 reports the phase-space dynamics of the diagonal and off-diagonal elements of the dispersion tensor $\sigma_{ij}^{(u,u)}$ under the different conditions.

We cannot observe a distinctive phase-space dynamic between the different conditions, which seem to be all characterized by a Brownian-like coverage of the phase-space [39]. However, it seems that particles move along outward and inward trajectories that becomes very irregular for long times. Furthermore, there are also no distinctive features between the diagonal and off-diagonal separations, thus suggesting the existence of a chaotic nature [39]. We further inspect the statistics of the dispersion tensor by looking at the average square

distances between elements $\ell^2 = \langle \sigma_{jj}^{(u_i)} \rangle$ as a function of the time steps under the different conditions. The results are reported in Figure 2.

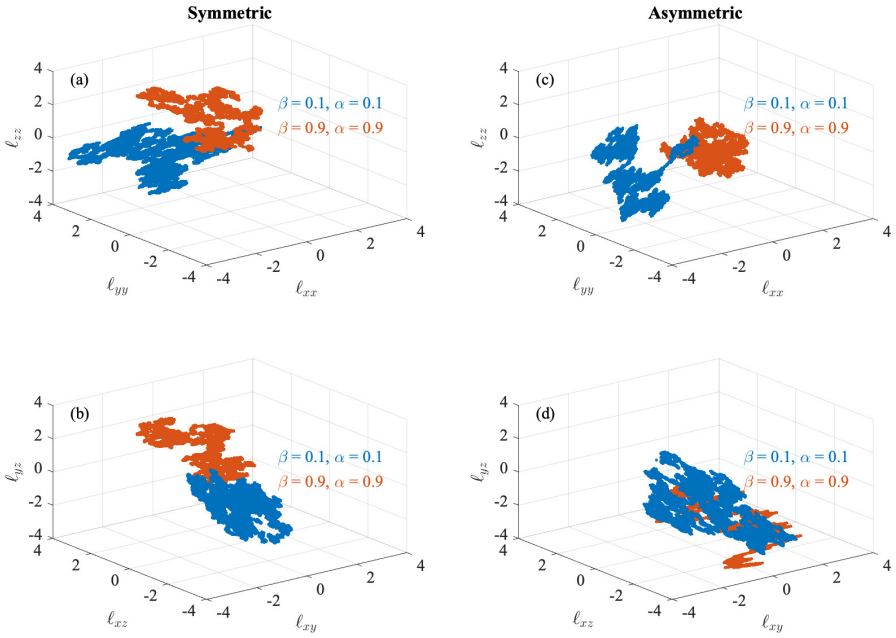

Figure 1. The phase-space dynamics of the diagonal (**a**) and off-diagonal (**b**) elements of the velocity dispersion tensor under the effect of symmetric field gradients $\gamma_i^j = \gamma =$ constant $\forall i, j$. (**c**,**d**) The same for the asymmetric field gradients. Blue and orange points refer to laminar and turbulent plasma environments, respectively. Axes are reported in units of standard deviations for clarity.

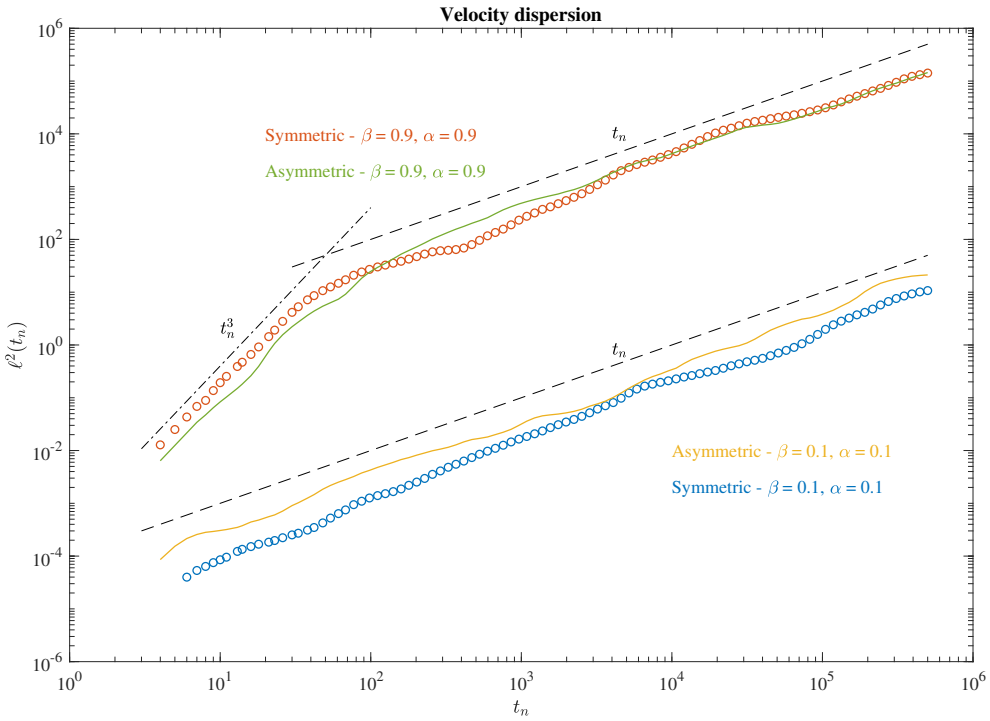

Figure 2. The average square distances between elements for the velocity dispersion as a function of the time steps. Dots refer to the symmetric field gradients, while lines refer to asymmetric field gradients. Orange and green correspond to turbulent conditions, while yellow and blue to laminar ones. The dashed-dotted line marks the Richardson scaling t_n^3, while the dashed line refers to the Brownian scaling t_n.

Here, a distinctive feature clearly emerges between laminar and turbulent plasmas. While the former are characterized by an uncorrelated path at all times, the latter are instead characterized by a Richardson scaling t^3 for short times, which transits towards a Brownian-like dispersion for long times. This behavior clearly reflects the existence of a spectral break separation in the Fourier PSD behavior, as previously reported by Alberti et al. [13] for turbulent conditions, being absent for laminar ones [13]. Indeed, an intermediate range of frequency is observed with a Kolmogorov-like spectral slope $-5/3$, followed by an f^{-1} behavior of large frequencies. The position of the scaling break for $\ell^2(t_n)$ is consistent with the location of the previously observed spectral break. This means that, despite its simplifications, the Lagrangian turbulence developed with a PMMHD model is in agreement with theoretical expectations from the Lagrangian counterpart of the Kolmogorov theory of turbulence, saying that the Richardson law can only be recovered and valid if an inertial sub-range of scales is observed [23,24]. As a further step, we investigated the anisotropic nature of the advection by looking at the anisotropy angles $\theta_{ij}^{(u_i,u_j)}$ under the different conditions, as reported in Figure 3.

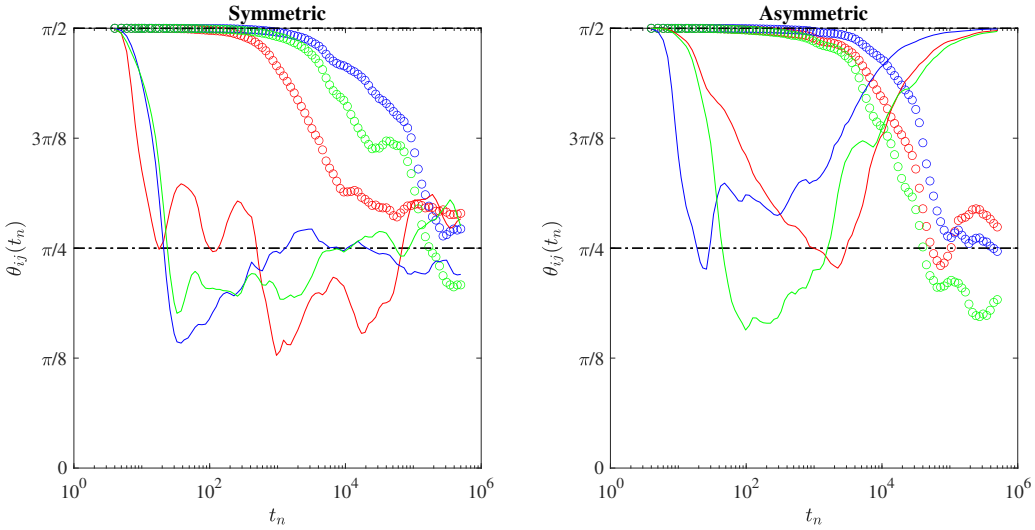

Figure 3. The anisotropy angles $\theta_{ij}^{(u_i,u_j)}$ as a function of the time steps. Dots refer to laminar conditions, while lines refer to turbulent ones. Red, green, and blue lines/symbols refer to θ_{xy}, θ_{xz}, and θ_{yz}, respectively. The dashed-dotted horizontal lines mark the purely isotropic advection condition $\theta_{ij} = \frac{\pi}{4}$.

The results look really intriguing. We clearly highlight that, after an initial transient activity, the chaotic advection of Lagrangian particles under turbulent conditions with symmetric field gradients becomes purely isotropic $\theta_{ij} = \pi/4$ (apart from some transient fluctuations), faster ($t_n \sim 10$) than the observed break ($t_n \sim 10^2$) associated with the Richardson scaling. Conversely, under asymmetric field gradients, it again becomes highly anisotropic for long times ($t_n \gtrsim 10^3$), which cannot be attributed to transient activity. This seems to underline that singularities in the field gradients along different directions can play a key role in destroying isotropy. Furthermore, when looking at laminar conditions, the anisotropy angles θ_{ij} behave in an almost similar way both for symmetric and asymmetric field gradients, thus suggesting that the loss of memory processes is the key driver of Lagrangian dispersion in non-turbulent environments. Our findings clearly highlight, with a simple model, a key property of turbulence, i.e., the mixing of chaotic trajectories [23].

6. Alfvénic Dispersion

The second case we study is the alfvénic dispersion, i.e., $s_i = b_i$, of particles. Figure 4 reports the phase-space dynamics of the diagonal and off-diagonal elements of the dispersion tensor $\sigma_{ij}^{(b,b)}$ under the different conditions.

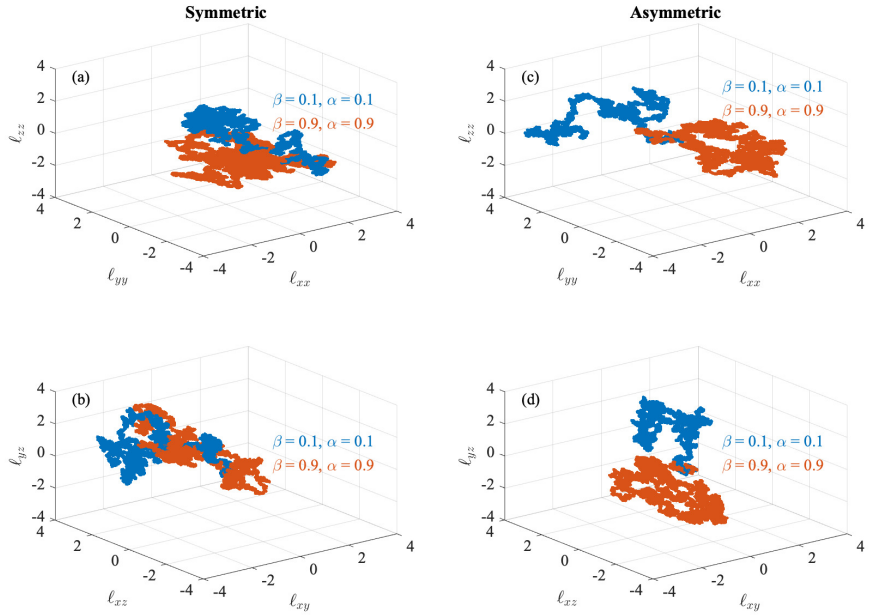

Figure 4. The phase-space dynamics of the diagonal (**a**) and off-diagonal (**b**) elements of the alfvénic dispersion tensor under the effect of symmetric field gradients $\gamma_i^j = \gamma =$ constant $\forall i, j$. (**c**,**d**) The same for the asymmetric field gradients. Blue and orange points refer to laminar and turbulent plasma environments, respectively. Axes are reported in units of standard deviations for clarity.

As for fluid velocity dispersion, there are no distinctive phase-space dynamics between the different conditions, which seem to all be characterized by a Brownian-like coverage of the phase-space [39]. However, more elongated structures are found for the symmetric case with respect to the asymmetric one, almost independent on the diagonal and off-diagonal separations. This seems to suggest that the magnetic field can play a role in ordering trajectories within a chaotic environment. We then inspect the statistics of the alfvénic dispersion tensor by looking at the average square distances between elements $\ell^2 = \langle \sigma_{jj}^{(b_i)} \rangle$ as a function of the time steps under the different conditions. The results are reported in Figure 5.

Again, here, a distinctive feature emerges between laminar and turbulent plasmas, independently of the topological properties of field gradients. Indeed, laminar conditions lead to a Brownian-like scaling for all times, while turbulent ones produce a short-term Richardson scaling and a long-term Brownian-like dispersion. This is, as for fluid dispersion, the Lagrangian counterpart of the Kolmogorov theory of turbulence, implying that the Richardson law exists if an inertial sub-range of scales is observed [23,24]. We further inspect the anisotropic nature of the advection by looking at the anisotropy angles $\theta_{ij}^{(b_i,b_j)}$ under the different conditions, as reported in Figure 6.

The results again look surprising. Indeed, we almost observe a similar behavior as fluid dispersion for laminar conditions, although it seems that isotropy is now recovered in a shorter time than that depicted for the fluid dispersion. Thus, the magnetic field also seems to produce faster isotropization of Lagrangian trajectories for laminar environments. In a similar way to fluid dispersion, after an initial transient activity, the chaotic advection of Lagrangian particles under turbulent conditions with symmetric field gradients becomes purely isotropic $\theta_{ij} = \pi/4$ (apart from some transient fluctuations), faster ($t_n \sim 10$) than the observed break ($t_n \sim 10^2$) associated with the Richardson scaling. The main difference with respect to the fluid dispersion is that, under asymmetric field gradients, the highly anisotropic behavior previously observed for long times ($t_n \gtrsim 10^3$) disappears. Thus, the magnetic field seems to be able to suppress the role of singularities in the field gradients along different directions and to restore isotropy. This confirms our initial thoughts on the ordering role of the magnetic field.

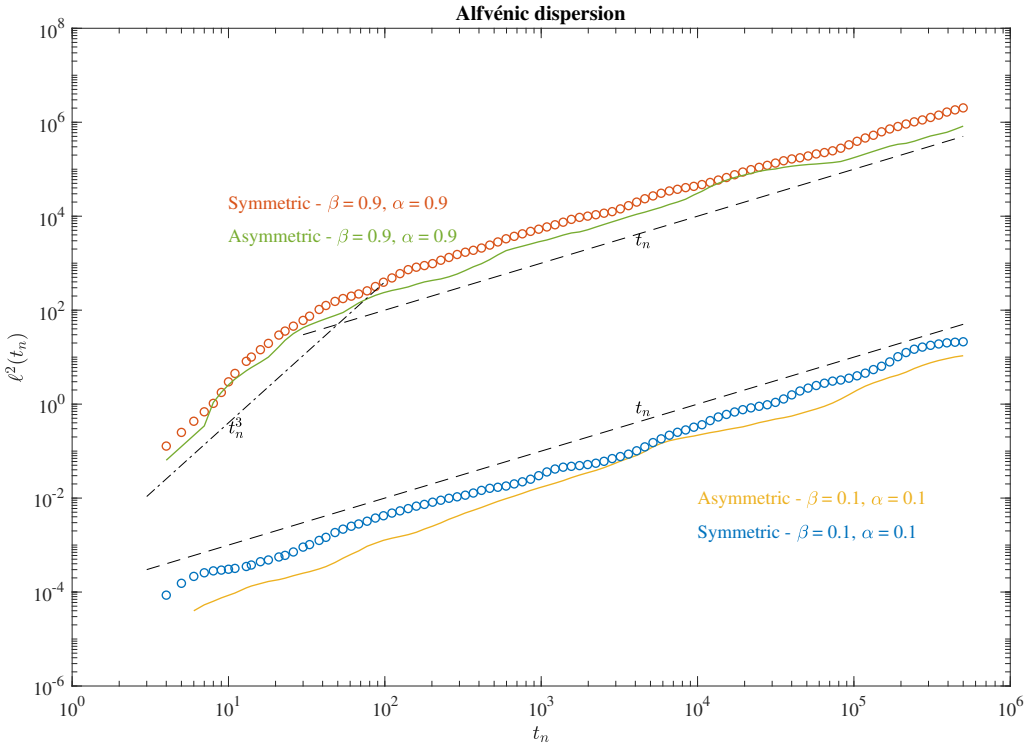

Figure 5. The average square distances between elements for the alfvénic dispersion as a function of the time steps. Dots refer to the symmetric field gradients, while lines refer to asymmetric field gradients. Orange and green correspond to turbulent conditions, while yellow and blue to laminar ones. The dashed-dotted line marks the Richardson scaling t_n^3, while the dashed line refers to the Brownian scaling t_n.

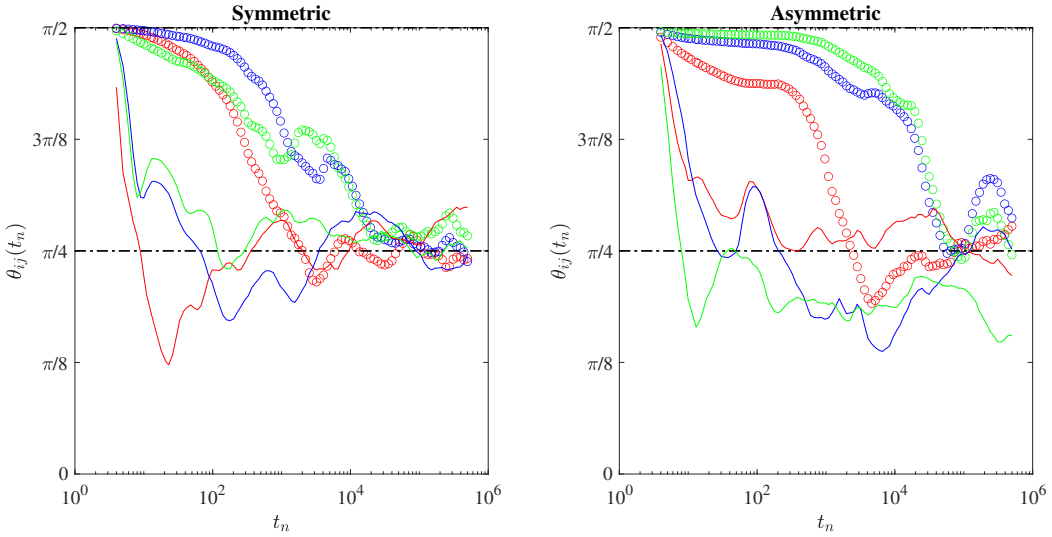

Figure 6. The anisotropy angles $\theta_{ij}^{(b_i,b_j)}$ as a function of the time steps. Dots refer to laminar conditions, while lines refer to turbulent ones. Red, green, and blue lines/symbols refer to θ_{xy}, θ_{xz}, and θ_{yz}, respectively. The dashed-dotted horizontal lines mark the purely isotropic advection condition $\theta_{ij} = \frac{\pi}{4}$.

7. Hydrodynamic Dispersion

The last case we study is the hydrodynamic dispersion, i.e., $s_i = u_i$ and $b_i = 0$, of particles, which the PMMHD model reduces to

$$\dot{u}_i = \beta_i u_i - \Gamma_i^j u_i u^j. \tag{29}$$

Figure 7 reports the phase-space dynamics of the diagonal and off-diagonal elements of the dispersion tensor $\sigma_{ij}^{(u,u|b=0)}$ under the different conditions.

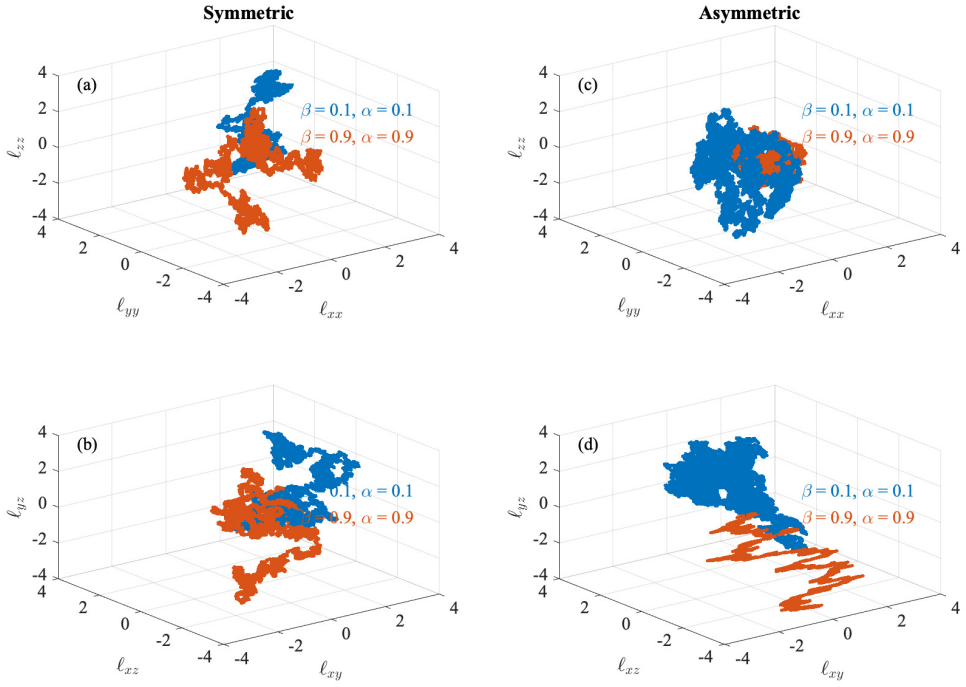

Figure 7. The phase-space dynamics of the diagonal (**a**) and off-diagonal (**b**) elements of the hydrodynamic dispersion tensor under the effect of symmetric field gradients $\gamma_i^j = \gamma =$ constant $\forall i, j$. (**c**,**d**) The same for the asymmetric field gradients. Blue and orange points refer to laminar and turbulent plasma environments, respectively. Axes are reported in units of standard deviations for clarity.

As for previous cases, we cannot highlight any distinctive feature of the phase-space dynamics between the different conditions. We then inspect the statistics of the hydrodynamic dispersion tensor by looking at the average square distances between elements $\ell^2 = \langle \sigma_{jj}^{(u,u|b=0)} \rangle$ as a function of the time steps under the different conditions. The results are reported in Figure 8.

For all conditions, the Richardson t^3-scaling disappears, with the presence of a Brownian-like scaling for all times. This result clearly suggests that the Lagrangian counterpart of the Kolmogorov theory of turbulence, implying that the Richardson law exists if an inertial sub-range of scales is observed, could no longer be valid for MHD turbulence, now requiring an additional condition. This condition is the existence of a magnetic field. However, this can be related to the reduced-order nature of the PMMHD model in the case $b = 0$. Indeed, by looking at Equation (29), it is easy to observe that it admits two different fixed points: one is the trivial solution ($u_i = 0$), and the other is $u^j = \frac{\beta_i}{\Gamma_i^j}$ [13]. The latter condition relates the equilibrium solution u_j with the parametrization of the spatial gradients Γ_i^j along perpendicular directions to the considered component, thus modifying the scaling for pair separation and likely destroying the correlations induced by the energy cascade. This could explain the missing of the Richardson t^3-scaling in the absence of a magnetic

field in our moodel, which is not usually observed in numerical simulations of pure fluid flows retaining more spatial modes, e.g., [34]. By further inspecting the anisotropic nature (see Figure 9), we recover similar results as for the fluid case.

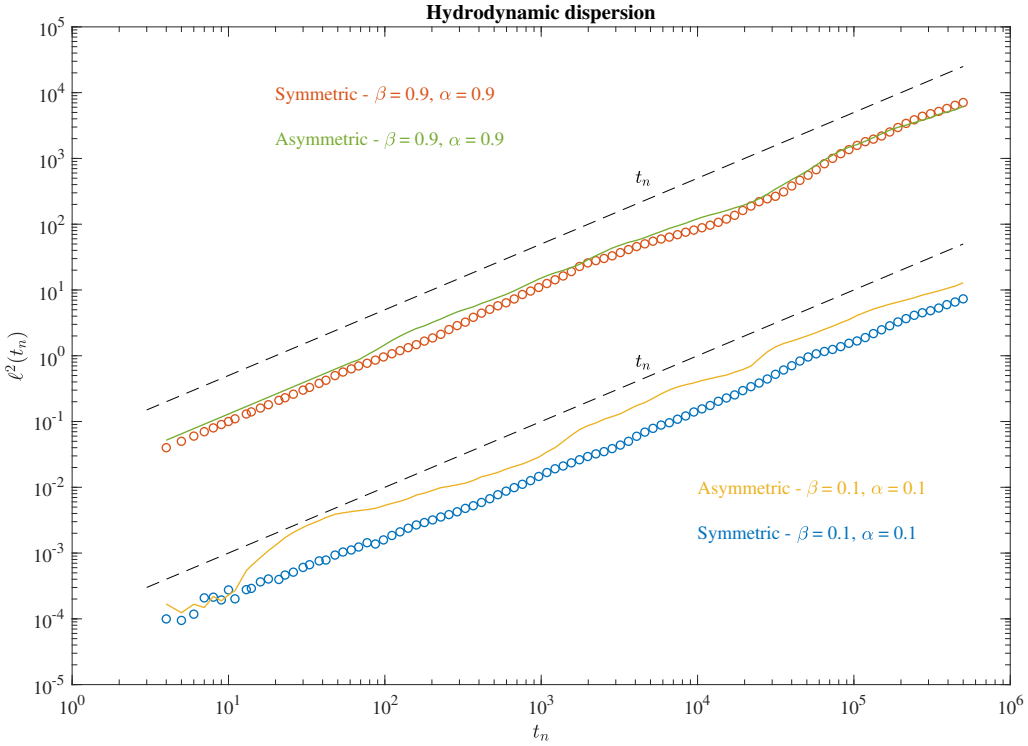

Figure 8. The average square distances between elements for the hydrodynamic dispersion as a function of the time steps. Dots refer to the symmetric field gradients, while lines refer to asymmetric field gradients. Orange and green correspond to turbulent conditions, while yellow and blue to laminar ones. The dashed lines refer to the Brownian scaling t_n.

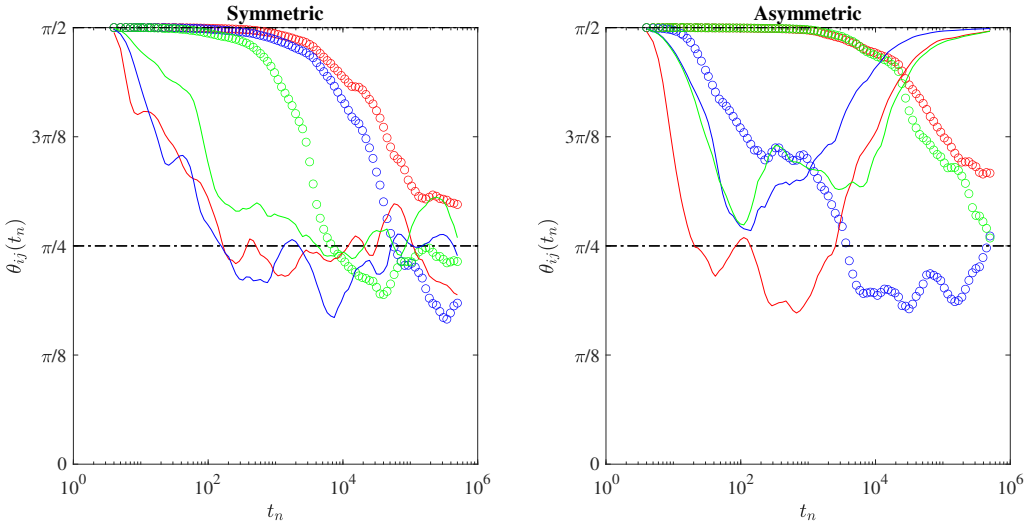

Figure 9. The anisotropy angles $\theta_{ij}^{(u_i,u_j|b_i=0)}$ as a function of the time steps. Dots refer to laminar conditions, while lines refer to turbulent ones. Red, green, and blue lines/symbols refer to θ_{xy}, θ_{xz}, and θ_{yz}, respectively. The dashed-dotted horizontal lines mark the purely isotropic advection condition $\theta_{ij} = \frac{\pi}{4}$.

This means that, after an initial transient activity, the chaotic advection of Lagrangian particles under turbulent conditions with symmetric field gradients and/or for laminar

plasmas becomes purely isotropic $\theta_{ij} = \pi/4$. Conversely, under asymmetric field gradients, it becomes again highly anisotropic for long times ($t_n \gtrsim 10^3$), which cannot be attributed to transient activity. This seems to underline again that the lack of a magnetic field allows singularities in the field gradients along different directions to play a key role in destroying isotropy. Furthermore, when looking at laminar conditions under asymmetric field gradients, we observe a shorter time for recovering isotropic conditions for the $y - z$ separation that can be attributed to the different lower value of γ_y^z for this setup with respect to γ_x^y and γ_x^z.

8. Summary and Conclusions

In this research, we investigate the dispersion of Lagrangian particles in synthetic velocity and magnetic fields created using the PMMHD model, considering both laminar and turbulent conditions. Our findings demonstrate distinct behaviors for each case.

Under laminar conditions, we observe that the average square distance between particle pairs shows a linear dependence on time, indicating Brownian-like dispersion throughout all time steps. Conversely, turbulent conditions exhibit a Richardson scaling pattern, resulting in super-ballistic dispersion. This scaling aligns with the anticipated properties for a turbulent environment and is particularly evident within the inertial sub-range of turbulence, as reproduced by the PMMHD model.

Furthermore, we find that in a turbulent environment, the magnetic field proves significantly more effective in dispersing particle pairs compared with the velocity field. However, in a laminar setting, no such differences are detected. Additionally, the velocity field generates stronger anisotropies than the magnetic field, suggesting an ordering influence of the magnetic field.

Finally, through an investigation of a purely hydrodynamic scenario where magnetic field effects are absent, we show that even in turbulent conditions, a Brownian-like behavior is observed. This indicates the crucial role of the magnetic field in generating the Richardson scaling observed in reduced-order models of turbulent environments. However, this can be related to a link between the equilibrium solution u_j and the parameterization of the spatial gradients Γ_i^j that could modify the scaling for pair separation and likely destroy the correlations induced by the energy cascade. This could be the explanation for the missing of the Richardson t^3-scaling in the absence of a magnetic field, which is not usually observed in numerical simulations retaining more spatial modes, e.g., [34]. However, this aspect is a claim for specific future investigations.

Our results are well in agreement with those reported by Carbone et al. [40] through a five-mode reduced-order model of two-dimensional MHD equations. Indeed, they have shown that in the presence of magnetic fluctuations, Lagrangian dispersion closely follows the standard Richardson description, while when magnetic fluctuations are excluded from the model, the Richardson regime is not observed and a Brownian-like behavior is observed [40]. Furthermore, they also reported a significant role of the intrinsic large-scale anisotropy of the model in affecting the direction of Lagrangian pair separation. Furthermore, we also recover similar results with those obtained using direct numerical simulations of anisotropic MHD turbulence [32], who reported scalings for relative Lagrangian dispersion in agreement with the Richardson prediction over the inertial sub-range and with a Brownian-like behavior for longer times. These aspects clearly highlight that, despite our drastic truncation of the MHD equations, our PMMHD model is able to reproduce similar results obtained via intermediate-to-high-complexity models, thus making it highly appropriate for utilization in scenarios where one needs synthetic turbulent fields with authentic characteristics, such as when conducting intricate investigations (e.g., sub-grid-scale models for MHD simulations). Clearly, our "one-scale" approach can open a novel framework for investigating the role of the ergodic nature of the synthetic field derived via the PMMHD model, which preserves temporal scaling properties (e.g., Kolmogorov-like spectra, Richardson dispersion), although neglecting the multiple spa-

tial scale nature of turbulent fields, thus being a promising outstanding (and additional) challenge in turbulence.

Author Contributions: Conceptualization, T.A. and V.C.; methodology, T.A.; software, T.A.; formal analysis, T.A.; investigation, V.C.; writing—original draft preparation, T.A. and V.C.; writing—review and editing, T.A. and V.C. All authors have read and agreed to the published version of the manuscript.

Funding: This research received no external funding.

Data Availability Statement: No data were created for this study.

Acknowledgments: We would like to sincerely acknowledge all the many collaborators, friends, and colleagues with whom we have interacted on the contents reported in this paper.

Conflicts of Interest: The authors declare no conflict of interest.

References

1. Biskamp, D. *Magnetohydrodynamic Turbulence*; Cambridge University Press: Cambridge, UK , 2003. [CrossRef]
2. Bruno, R.; Carbone, V. *Turbulence in the Solar Wind*; Springer: Berlin/Heidelberg, Germany, 2016; Volume 928.
3. Canuto, V.M.; Christensen-Dalsgaard, J. TURBULENCE IN ASTROPHYSICS: Stars. *Annu. Rev. Fluid Mech.* **1998**, *30*, 167–198. [CrossRef]
4. Hersant, F.; Dubrulle, B.; Huré, J.M. Turbulence in circumstellar disks. *Astron. Astrophys.* **2005**, *429*, 531–542. [CrossRef]
5. Brandenburg, A.; Nordlund, A. Astrophysical turbulence. *Rep. Prog. Phys.* 2011, *74*, 046901. [CrossRef]
6. McKee, C.; Stone, J. Turbulence in the heavens. *Nat. Astron.* **2021**, *5*, 342–343. [CrossRef]
7. Valentini, F.; Servidio, S.; Perrone, D.; Califano, F.; Matthaeus, W.H.; Veltri, P. Hybrid Vlasov-Maxwell simulations of two-dimensional turbulence in plasmas. *Phys. Plasmas* **2014**, *21*, 082307. [CrossRef]
8. Oughton, S.; Matthaeus, W.H.; Wan, M.; Parashar, T. Variance anisotropy in compressible 3-D MHD. *J. Geophys. Res. (Space Phys.)* **2016**, *121*, 5041–5054. [CrossRef]
9. Pezzi, O.; Parashar, T.N.; Servidio, S.; Valentini, F.; Vásconez, C.L.; Yang, Y.; Malara, F.; Matthaeus, W.H.; Veltri, P. Revisiting a Classic: The Parker-Moffatt Problem. *Astrophys. J.* **2017**, *834*, 166. [CrossRef]
10. Piron, L.; Bonfiglio, D.; Piovesan, P.; Zaniol, B.; Auriemma, F.; Carraro, L.; Chacón, L.; Marrelli, L.; Valisa, M.; Veranda, M.; et al. 3D magnetic fields and plasma rotation in RFX-mod tokamak plasmas. *Nucl. Fusion* **2013**, *53*, 113022. [CrossRef]
11. Poli, F.M. Integrated Tokamak modeling: When physics informs engineering and research planning. *Phys. Plasmas* **2018**, *25*, 055602. [CrossRef]
12. Bandyopadhyay, R.; Matthaeus, W.H.; Parashar, T.N. Single-mode nonlinear Langevin emulation of magnetohydrodynamic turbulence. *Phys. Rev. E* **2018**, *97*, 053211. [CrossRef]
13. Alberti, T.; Consolini, G.; Carbone, V. A discrete dynamical system: The poor man's magnetohydrodynamic (PMMHD) equations. *Chaos* **2019**, *29*, 103107. [CrossRef] [PubMed]
14. Alexandrova, O.; Jagarlamudi, V.K.; Hellinger, P.; Maksimovic, M.; Shprits, Y.; Mangeney, A. Spectrum of kinetic plasma turbulence at 0.3-0.9 astronomical units from the Sun. *Phys. Rev. E* **2021**, *103*, 063202. [CrossRef] [PubMed]
15. Carbone, V.; Lepreti, F.; Vecchio, A.; Alberti, T.; Chiappetta, F. On the origin of high-frequency magnetic fluctuations in the interplanetary medium: A Brownian-like approach. *Front. Phys.* **2021**, *9*, 18. [CrossRef]
16. Carbone, V.; Telloni, D.; Lepreti, F.; Vecchio, A. High-frequency Magnetic Fluctuations in Space Plasmas and the Role of Electron Landau Damping. *Astrophys. J. Lett.* **2022**, *924*, L26. [CrossRef]
17. Cho, J.; Lazarian, A. Particle Acceleration by Magnetohydrodynamic Turbulence. *Astrophys. J.* **2006**, *638*, 811. [CrossRef]
18. Lemoine, M. Particle acceleration in strong MHD turbulence. *Phys. Rev. D* **2021**, *104*, 063020. [CrossRef]
19. Kolmogorov, A. The Local Structure of Turbulence in Incompressible Viscous Fluid for Very Large Reynolds' Numbers. *Akad. Nauk SSSR Dokl.* **1941**, *30*, 301–305.
20. Iroshnikov, P.S. Turbulence of a Conducting Fluid in a Strong Magnetic Field. *Sov. Ast.* **1964**, *7*, 566.
21. Kraichnan, R.H. Inertial-Range Spectrum of Hydromagnetic Turbulence. *Phys. Fluids* **1965**, *8*, 1385–1387. [CrossRef]
22. Borgas, M.S. The Multifractal Lagrangian Nature of Turbulence. *Philos. Trans. R. Soc. Lond. Ser. A* **1993**, *342*, 379–411. [CrossRef]
23. Benzi, R.; Biferale, L.; Calzavarini, E.; Lohse, D.; Toschi, F. Velocity-gradient statistics along particle trajectories in turbulent flows: The refined similarity hypothesis in the Lagrangian frame. *Phys. Rev. E* **2009**, *80*, 066318. [CrossRef]
24. Bentkamp, L.; Lalescu, C.C.; Wilczek, M. Persistent accelerations disentangle Lagrangian turbulence. *Nat. Commun.* **2019**, *10*, 3550. [CrossRef] [PubMed]
25. Carbone, V. Cascade model for intermittency in fully developed magnetohydrodynamic turbulence. *Phys. Rev. Lett.* **1993**, *71*, 1546–1548. [CrossRef] [PubMed]
26. Chillà, F.; Peinke, J.; Castaing, B. Multiplicative Process in Turbulent Velocity Statistics: A Simplified Analysis. *J. Phys. II* **1996**, *6*, 455–460. [CrossRef]

27. Dubrulle, B. Intermittency in fully developed turbulence: Log-Poisson statistics and generalized scale covariance. *Phys. Rev. Lett.* **1994**, *73*, 959–962. [CrossRef] [PubMed]
28. Laval, J.P.; Dubrulle, B. A LES-Langevin model for turbulence. *Eur. Phys. J. B* **2006**, *49*, 471–481. [CrossRef]
29. Schertzer, D.; Lovejoy, S. Generalised scale invariance in turbulent phenomena. *PhysicoChemical Hydrodyn.* **1985**, *6*, 623–635.
30. Monin, A.S.; Yaglom, A.M.; Ablow, C.M. Statistical Fluid Mechanics: The Mechanics of Turbulence. *Am. J. Phys.* **1977**, *45*, 1010. [CrossRef]
31. Toschi, F.; Bodenschatz, E. Lagrangian Properties of Particles in Turbulence. *Annu. Rev. Fluid Mech.* **2009**, *41*, 375–404. [CrossRef]
32. Pratt, J.; Busse, A.; Müller, W.C. Reynolds number dependence of Lagrangian dispersion in direct numerical simulations of anisotropic magnetohydrodynamic turbulence. *J. Fluid Mech.* **2022**, *944*, A36. [CrossRef]
33. Richardson, L.F. Atmospheric diffusion shown on a distance-neighbour graph. *Proc. R. Soc. London. Ser. A Contain. Pap. A Math. Phys. Character* **1926**, *110*, 709–737.
34. Salazar, J.P.L.C.; Collins, L.R. Two-Particle Dispersion in Isotropic Turbulent Flows. *Annu. Rev. Fluid Mech.* **2009**, *41*, 405–432. [CrossRef]
35. Thalabard, S.; Krstulovic, G.; Bec, J. Turbulent pair dispersion as a continuous-time random walk. *J. Fluid Mech.* **2014**, *755*, R4. [CrossRef]
36. Bourgoin, M. Turbulent pair dispersion as a ballistic cascade phenomenology. *J. Fluid Mech.* **2015**, *772*, 678–704. [CrossRef]
37. Elsinga, G.; Ishihara, T.; Hunt, J. Non-local dispersion and the reassessment of Richardson's t3-scaling law. *J. Fluid Mech.* **2022**, *932*, A17. [CrossRef]
38. McDonough, J.M. Three-dimensional poor man's Navier-Stokes equation: A discrete dynamical system exhibiting $k^{-5/3}$ inertial subrange energy scaling. *Phys. Rev. E* **2009**, *79*, 065302. [CrossRef]
39. Wang, L.P.; Maxey, M.R.; Burton, T.D.; Stock, D.E. Chaotic dynamics of particle dispersion in fluids. *Phys. Fluids A Fluid Dyn.* **1992**, *4*, 1789–1804. [CrossRef]
40. Carbone, F.; Telloni, D.; Zank, G.; Sorriso-Valvo, L. Chaotic advection and particle pairs diffusion in a low-dimensional truncation of two-dimensional magnetohydrodynamics. *EPL Europhys. Lett.* **2022**, *138*, 53001. [CrossRef]